

The dependence of oxygen vacancy distributions in BiFeO₃ films on oxygen pressure and substrate

G. L. Yuan,¹ L. W. Martin,² R. Ramesh,^{2,3} and A. Uedono^{1,a)}

¹*Institute of Applied Physics, Graduate School of Pure and Applied Sciences, University of Tsukuba, Tsukuba, Ibaraki 305-8573, Japan*

²*Materials Science Division, Lawrence Berkeley National Laboratory, Berkeley, California 94720, USA*

³*Departments of Materials Science and Engineering and Physics, University of California-Berkeley, Berkeley, California 94720, USA*

(Received 31 May 2009; accepted 16 June 2009; published online 7 July 2009)

The epitaxial (001)-oriented 250 nm BiFeO₃/50 nm SrRuO₃ films were deposited on DyScO₃ and SrTiO₃ substrates, respectively. Following the growth, the cooling in lower oxygen pressure results in the creation of oxygen vacancies at the surface of the BiFeO₃ film and the epitaxial strain drives these vacancies to diffuse from the film surface to the film interface. The SrTiO₃ substrate strongly absorbs oxygen vacancies from the BiFeO₃ film while the DyScO₃ substrate does not. Therefore, the depth distribution of oxygen vacancies depends on the oxygen pressure during cooling, the epitaxial strain, and the substrate absorbing oxygen vacancies. © 2009 American Institute of Physics.

[DOI: 10.1063/1.3171939]

The study of oxygen vacancies (V_{O}) is very important for dielectric, ferroelectric, piezoelectric, or multiferroic $\text{ABO}_{3-\delta}$ (δ expresses the density of V_{O}) oxides that can be used in microelectronics, sensors, and other devices.¹⁻⁴ On one hand, even a low density of V_{O} may greatly increase leakage currents, relax strain, or even diminish ferroelectric properties in epitaxial BiFeO_{3- δ} films.²⁻⁴ On the other hand leaky BiFeO_{3- δ} also shows many wonderful properties such as photovoltaic effect.¹ Although these V_{O} in intergap states have been extensively studied,⁵⁻⁷ the mechanism of the formation of low-density distributions of V_{O} is not clear in BiFeO_{3- δ} and SrTiO_{3- δ} .

Positron annihilation, on the other hand, can nondestructively trace the depth-profile (from surface to $>1 \mu\text{m}$) distribution of such low-density vacancies. A positron can annihilate with an electron in heterostructures, emitting two γ rays with the energy (E_γ) of $\sim 511 \text{ keV}$. With a monoenergetic positron beam, the parameter (S) of positron annihilation can be measured as a function of the incident positron energy (E , keV), where S is defined as $S = N_s/N_T$, and N_T and N_s are the numbers of annihilation events occurring in the range of $503.8 \text{ keV} \leq E_\gamma \leq 518.2 \text{ keV}$ or $510.24 \text{ keV} \leq E_\gamma \leq 511.76 \text{ keV}$, respectively.⁸⁻¹² Compared with the S of vacancy-free material, the S of a material may increase when open volume and/or density of vacancy-type defects increase.⁸⁻¹²

In this article, we have found that the partial pressure of oxygen (P_{O_2}) during cooling after growth, strain-state, and substrate material are very important in manipulating the density, diffusion, and distribution of V_{O} .

Using pulsed laser deposition, 250 nm BiFeO_{3- δ} (BFO) and 50 nm SrRuO_{3- δ} (SRO) films (used as a bottom electrode) were epitaxially grown on (110)-DyScO_{3- δ} (DSO, starting $\delta \sim 0$) and (001)-SrTiO₃ (STO, starting $\delta \sim 0$) single crystal substrates at 700 °C and 0.1 Torr P_{O_2} .^{2,3,13} Following growth, these samples were then cooled to room temperature

at 5 °C/min in 760, 0.1, or 0.001 Torr P_{O_2} in order to induce different δ for BiFeO_{3- δ} , SrRuO_{3- δ} , or SrTiO_{3- δ} . Henceforth, we will refer to these samples as 760-, 0.1-, and 0.001-BFO/SRO/STO; and 760-, 0.1-, and 0.001-BFO/SRO/DSO. The crystal structure and strain of the samples were studied using x-ray diffraction (XRD). The density and distribution of V_{O} was estimated by positron annihilation. The S was analyzed by the VEPFIT method $S(E) = S_s F_s(E) + \sum S_i F_i(E)$ and $F_s(E) + \sum F_i(E) = 1$, where $F_s(E)$ is the fraction of positrons annihilated at the surface and $F_i(E)$ is that in the i th layer, S_s and S_i are the S parameters corresponding, respectively, to the annihilation of positrons on the surface and that in the i th layer.⁹⁻¹² Three layers were chosen for all samples except two layers for 0.1-BFO/SRO/STO, and one fixed boundary at 300 nm was used during simulation. BFO surfaces were studied using atomic force microscopy (AFM) and ferroelectric domains of the BFO films were studied using piezoelectric force microscopy (PFM). Other electric properties of similar samples were already reported in Refs. 2 and 3.

The evolution of strain in the BFO/SRO/DSO and BFO/SRO/STO heterostructures was studied by XRD patterns in Fig. 1. When there is no epitaxial strain, the pseudocubic crystal lattice is $\sim 0.3922 \text{ nm}$ for SRO ($\delta \sim 0$) thick film, $\sim 0.3906 \text{ nm}$ for STO ($\delta \sim 0$) crystal substrate, $\sim 0.3948 \text{ nm}$ for DSO ($\delta \sim 0$) crystal substrate, and $\sim 0.3965 \text{ nm}$ for BFO ($\delta \sim 0$) crystal.¹³⁻¹⁵ The 002 diffraction peaks of the BFO film were observed at larger angles for BFO/SRO/DSO in Fig. 1(a) compared to those of BFO/SRO/STO in Fig. 1(b), providing evidence for smaller compressive strain in BFO films of BFO/SRO/DSO than those of BFO/SRO/STO. For 760- and 0.1-BFO/SRO/DSO (or 0.001-BFP/SRO/DSO), the 002 diffraction peaks of BFO film are slightly higher than (or close to) the 45.770° expected for BFO ($\delta \sim 0$) crystal [inset of Fig. 1(a)], suggesting that the 250 nm BFO films are weakly strained (or is essentially relaxed by a higher δ). This suggestion is consistent with the fact that the full width at half maximum (FWHM) of 002 diffraction peak of DSO is narrowest in 0.001-BFP/SRO/DSO. For 760-, 0.1-, and 0.001-BFO/SRO/STO in the inset of Fig. 1(b), the 002 dif-

^{a)}Author to whom correspondence should be addressed. Electronic mail: uedono@sakura.cc.tsukuba.ac.jp.

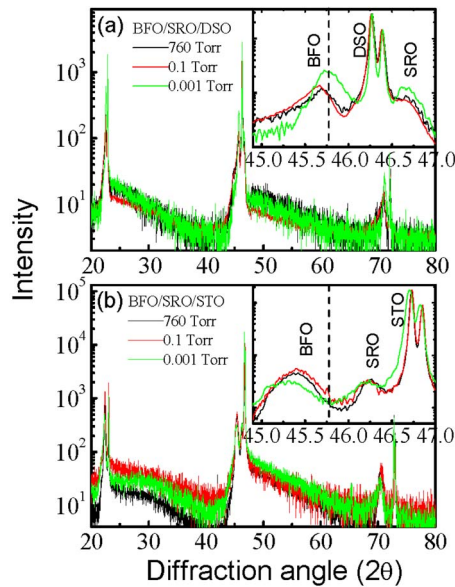


FIG. 1. (Color online) XRD patterns for (a) BFO/SRO/DSO and (b) BFO/SRO/STO, where the 002 peaks are amplified in insets and the dashed lines located at 45.770° expected for bulklike BFO.

fraction peaks of BFO films can be fitted by a peak with $2\theta_{002} \leq 45.390^\circ$, i.e., c axis of >0.3996 nm, which suggests that the density of V_{OS} is not high enough to effectively relax the compressive strain between the BFO film and the STO substrate in all BFO/STO/STO samples. Besides, the STO layer of 0.001-BFO/SRO/STO shows a little larger $2\theta_{002}$ and FWHM than those of 760-, 0.1-BFO/SRO/STO, suggesting that a large amount of V_{OS} diffused to STO, and then induced the lightly expanded c axis. This chemical expansion should relate to the increasing ionic radii of Ti ions with decreasing oxidation state from +4 to +3.¹⁶

In Fig. 2, the S - E curves of the three BFO/SRO/DSO and three BFO/SRO/STO heterostructures can be treated as

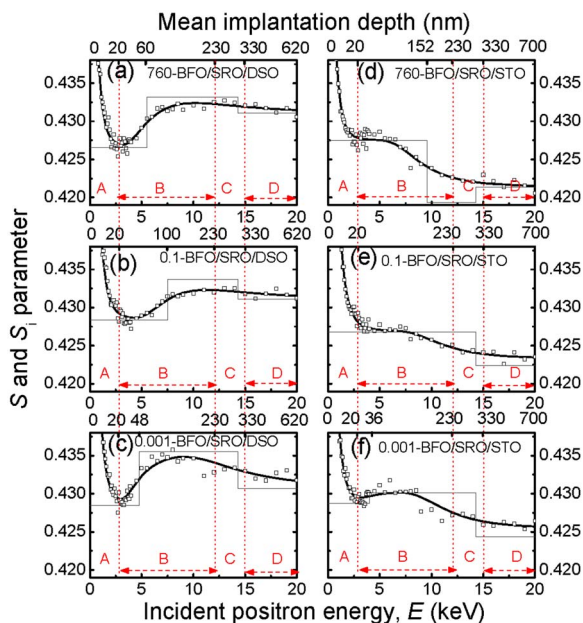


FIG. 2. (Color online) The S - E curves (open square), their simulations using VEPFIT method (black line for fitting S and gray lines for the estimated characteristic S of each layer), and the four regions divided by red dot lines of (a) 760-, (b) 0.1-, (c) 0.001-BFO/SRO/DSO, and (d) 760-, (e) 0.1-, and (f) 0.001-BFO/SRO/STO.

four regions as a whole. A mean implantation depth (Z , nanometer) can be estimated according to $Z = 27.5 \cdot E^{1.7} / \rho$ (unit of ρ is g/cm^3),^{9,10} for example, $Z = 240$ nm for 12.5 keV and $Z = 330$ nm for 15 keV. The highest S value observed at $E < 2.7$ keV (i.e., region A with Z between 0 and 20 nm) is mainly contributed by surface effects because some positrons implanted to the near-surface BFO can be reflected back and then annihilate at the surface. The S show a lowest value or turning point at ~ 2.7 keV, suggesting that the surface effect can be ignored at $E > 2.7$ keV. The S value at E ranging from ~ 2.7 to ~ 12 keV (i.e., region B with Z between 20 and 230 nm) is mostly contributed by BFO film and can be treated as the characteristic S of BFO (i.e., S_{BFO}). The S value at E between 12 and 15 keV (i.e., region C with Z between 230 and 330 nm, compared with Z between 250 and 300 nm for SRO layer) maybe be cocontributed by BFO, SRO, or substrate, where the boundaries of $E > 12$ and $E < 15$ keV are roughly estimated and their precision do not influence the following analyses. The S value at $E > 15$ keV (i.e., region D with $Z > 330$ nm) is contributed by substrate and it can be treated as the characteristic S of STO (i.e., S_{STO}) or DSO (i.e., S_{DSO}). The characteristic S value of BFO, SRO, DSO, and STO were also roughly estimated by VEPFIT method and the results were also shown in Fig. 2 for comparison. Therefore, the S value at regions B and D can be treated as S_{BFO} , S_{STO} , or S_{DSO} directly, and the large fluctuation of S_{BFO} in the B region suggests that the distribution of V_{OS} is not homogenous in BFO films.

For the three BFO/SRO/DSO heterostructures [Figs. 2(a)–2(c)], the distributions of V_{OS} in the BFO films can be explained according to the cooling P_{O_2} and strain. The S_{DSO} at region D is ~ 0.431 for 760-, 0.1-, and 0.001-BFO/SRO/DSO, suggesting that DSO absorbs few V_{OS} from the BFO/SRO films regardless of the variation in P_{O_2} from 760 to 0.001 Torr. This is consistent with the previous report that the highest breakdown field of 8 MV/cm was obtained in 10-nm-thick DyScO_3 films grown on Nb-SrTiO_3 substrate at $P_{\text{O}_2} = 0.001$ Torr.¹⁷ For DSO, the Dy/Sc just allows the $\text{Dy}^{3+}/\text{Sc}^{3+}$ ion as its stable ionic state, thus charge equilibrium cannot be kept when V_{OS} were produced or diffused in DyScO_3 . For S_{BFO} at B region, the S_{BFO} at $E \sim 2.7$ keV is lower than the S_{BFO} that extends to $E \sim 12$ keV, which should partially relate to the stronger strain of near-interface BFO. All vacancies feel a driving force to diffuse from near the BFO surface to near the BFO/SRO interface in order to lower the compressive-strain-induced elastic energy of the system.¹⁸

For the 760-BFO/SRO/STO heterostructure [Fig. 2(d)], the S_{BFO} at $E \sim 12$ keV is lower than the S_{BFO} at $E \sim 2.7$ keV in region B, and the S_{STO} is lower than the other two S_{STO} of 0.1- and 0.01-BFO/SRO/STO in region D. Although the stronger compressive strain in 760-BFO/SRO/STO should induce V_{OS} to diffuse from the BFO surface to the BFO/SRO interface, the variation between 760-BFO/SRO/STO and 760-BFO/SRO/DSO should not only come from their different strain-states as set by the substrate. The S_{STO} in region D increases as the cooling P_{O_2} is lowered from 760 to 0.001 Torr in the three BFO/SRO/STO, suggesting that the STO substrate does absorb V_{OS} from BFO/SRO films. It suggests that STO owes a lower energy of oxygen vacancies formation than that of DSO. Ti atoms allow Ti^{3+} and Ti^{4+} as their stable ion states, thus the transformation

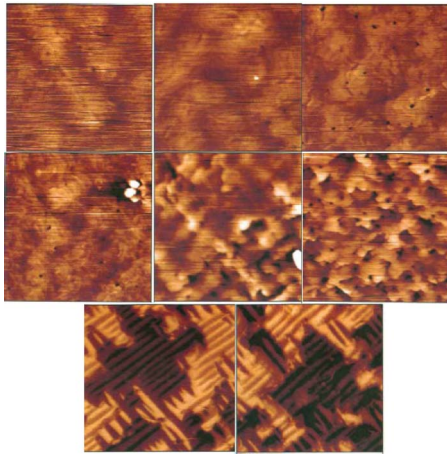


FIG. 3. (Color online) The AFM surface images of (a) 760-, (b) 0.1-, (c) 0.001-BFO/SRO/DSO, (d) 760-, (e) 0.1-, and (f) 0.001-BFO/SRO/STO, and the PFM in-plane images of (g) 0.1-BFO/SRO/DSO and (h) 0.1-BFO/SRO/STO, where all images are $5 \mu\text{m}^2$ and all AFM images have a height scale of 5 nm.

from Ti^{4+} to Ti^{3+} was induced to keep charge equilibrium when V_{O} s were produced. Therefore, the near-interface BFO layer is found to lose a large proportion of the V_{O} s due to STO absorbing V_{O} s in the 760-BFO/SRO/STO heterostructure since not enough V_{O} s were produced at BFO surface to offset such a loss. As a result the bottom BFO layer shows the lowest S_{BFO} at B region.

For the 0.1-BFO/SRO/STO heterostructure [Fig. 2(e)], S_{BFO} at $E \sim 2.7$ keV change a little, while both the S_{BFO} at $E \sim 12$ keV in region B and the S_{STO} in region D obviously increase compared with those in 760-BFO/SRO/STO. The STO appears to have absorbed many V_{O} s from the near-interface BFO to increase its S_{STO} . At the same time it appears that a nearly equal amount of V_{O} s were created at the BFO surface because of the decrease in P_{O_2} . Finally, these surface V_{O} s are thought to have diffused to the near-interface BFO because of the strong compressive strain from the STO substrate.

For the 0.001-BFO/SRO/STO heterostructure [Fig. 2(f)], the S_{BFO} in B region and S_{STO} in region D are higher than the corresponding S_{BFO} and S_{STO} in 760 and 0.1-BFO/SRO/STO [Figs. 2(d) and 2(e)]. The low cooling P_{O_2} (0.001 Torr) induced a large amount of V_{O} s to form at the surface of the BFO, which then diffuse to the near-interface BFO layer and the STO substrate. However, the S_{BFO} in B region and S_{STO} in region D are far lower than those of the strain-relaxed 0.001-BFO/SRO/DSO, thus the density of V_{O} s in BFO are not high enough to relax the strain between BFO and STO which is also confirmed by XRD pattern (Fig. 1).

The topographies of BFO surface relate to the S_{BFO} in B region and the S_{STO} or S_{DSO} in region D. Lower P_{O_2} during cooling worsens the surface of the BFO film for the three BFO/SRO/DSO heterostructures [Figs. 3(a)–3(c)]. When the films were cooled at lower P_{O_2} , more V_{O} s form in BFO/SRO films and more O_2 are evolved from the BFO surface. V_{O} s change the crystal structure and therefore change the surface morphology of BFO films. At 760, 0.1, or 0.001 Torr cooling P_{O_2} , BFO/SRO/STO heterostructure [Figs. 3(d)–3(f)] shows worse BFO surfaces than BFO/SRO/DSO, respectively. Further, decreasing the cooling P_{O_2} also worsens the BFO surface of BFO/SRO/STO faster than that of BFO/SRO/DSO.

For BFO/SRO/STO, their rougher surface should be due to their differences from BFO/SRO/DSO, i.e., the stronger compressive strain and/or the STO absorbing V_{O} s. As mentioned before, with the P_{O_2} decreasing from 760 to 0.001 Torr, BFO surface creates a large amount of V_{O} to satisfy the increased S_{STO} in region D.^{9,10} Simultaneously, a large amount of oxygen atoms in STO substrate diffused to BFO surface and contribute more O_2 . These V_{O} s diffusion, together with the V_{O} s-induced crystal expansion, should be the main reason of the BFO surface worsening.

In PFM in-plane images, all BFO films studied were found to show similar ferroelectric domain structures. As an example, in-plane PFM images of 0.1-BFO/SRO/DSO and 0.1-BFO/SRO/STO are shown in Figs. 3(g) and 3(h), respectively.

During the cooling of the sample, the lower partial pressure P_{O_2} helps the BFO surface to create additional V_{O} s, the epitaxial strain from substrate always drive these V_{O} s to the BFO/SRO interface, the STO substrate strongly absorb V_{O} s from BFO films in BFO/SRO/STO samples while DSO substrate does not absorb V_{O} s in BFO/SRO/DSO samples. The above three reasons contribute to several different depth distributions of V_{O} s and different surface roughness that can influence application of BFO films.

We thank S.Q. Chen and K. Akimoto for XRD measurement, and Yuan was supported by Japan Society for the Promotion of Science (JSPS) in Tsukuba University. The work at LBNL and Berkeley was supported by the U.S. Department of Energy under Contract No. DE-AC0205CH11231.

- ¹T. Choi, S. Lee, Y. J. Choi, V. Kiryukhin, and S.-W. Cheong, *Science* **324**, 63 (2009).
- ²G. W. Pabst, L. W. Martin, Y. H. Chu, and R. Ramesh, *Appl. Phys. Lett.* **90**, 072902 (2007).
- ³S. R. Basu, L. W. Martin, Y. H. Chu, M. Gajek, R. Ramesh, R. C. Rai, X. Xu, and J. L. Musfeldt, *Appl. Phys. Lett.* **92**, 091905 (2008).
- ⁴A. Kalubukhov, R. Gunnarsson, J. Borjesson, E. Olsson, T. Claesson, and D. Winkler, *Phys. Rev. B* **75**, 121404(R) (2007).
- ⁵D. D. Cuong, B. Lee, K. M. Choi, H. S. Ahn, S. Han, and J. Lee, *Phys. Rev. Lett.* **98**, 115503 (2007).
- ⁶F. Cordero, *Phys. Rev. B* **76**, 172106 (2007).
- ⁷C. Ederer and N. A. Spaldin, *Phys. Rev. B* **71**, 224103 (2005).
- ⁸D. J. Keeble, B. Nielsen, A. Krishnan, K. G. Lynn, S. Madhukar, R. Ramesh, and C. F. Yong, *Appl. Phys. Lett.* **73**, 318 (1998).
- ⁹A. Uedono, K. Shimayama, M. Kiyohara, Z. Q. Chen, and K. Yamabe, *J. Appl. Phys.* **92**, 2697 (2002).
- ¹⁰A. Uedono, Z. Q. Chen, K. Yamabe, T. Ohdaira, R. Suzuki, and T. J. Mikado, *J. Appl. Phys.* **91**, 5307 (2002).
- ¹¹S. McGuire, D. J. Keeble, R. E. Mason, P. G. Coleman, Y. Koutsonas, and T. J. Jackson, *J. Appl. Phys.* **100**, 044109 (2006).
- ¹²A. van Veen, H. Schut, M. Clement, J. M. M. de Nijs, A. Kruseman, and M. R. Ijzma, *Appl. Surf. Sci.* **85**, 216 (1995).
- ¹³Y. H. Chu, Y.-H. Chu, Q. Zhan, L. W. Martin, M. P. Cruz, P. L. Yang, G. W. Pabst, F. Zavaliiche, S. Y. Yang, J. X. Zhang, L. Q. Chen, D. G. Schlom, I. N. Lin, T. B. Wu, and R. Ramesh, *Adv. Mater.* **18**, 2307 (2006).
- ¹⁴J. Wang, J. B. Neaton, H. Zheng, V. Nagarajan, S. B. Ogale, B. Liu, D. Viehland, V. Vaithyanathan, D. G. Schlom, U. V. Waghmare, N. A. Spaldin, K. M. Rabe, M. Wuttig, and R. Ramesh, *Science* **299**, 1719 (2003).
- ¹⁵T. Zhao, A. Scholl, F. Zavaliiche, K. Lee, M. Barry, A. Doran, M. P. Cruz, Y. H. Chu, C. Ederer, N. A. Spaldin, R. R. Das, D. M. Kim, S. H. Baek, C. B. Eom, and R. Ramesh, *Nature Mater.* **5**, 823 (2006).
- ¹⁶A. Fossdal, M. Menon, I. Waernhus, K. Wiik, M. A. Einarsrud, and T. Grande, *J. Am. Ceram. Soc.* **87**, 1952 (2004).
- ¹⁷T. Uozumi, K. Shibuya, T. Ohnishi, T. Sato, and M. Lippmaa, *Jpn. J. Appl. Phys., Part 2* **45**, L830 (2006).
- ¹⁸R. Poyato, M. L. Calzada, and L. Pardo, *Appl. Phys. Lett.* **86**, 042905 (2005).